Int j simul model 21 (2022) 2, 320-331
Original scientific paper

FATIGUE-LIFE EVALUATION METHOD FOR RING-WELDED JOINTS

Yang, L.; Yang, B.; Yang, G. W.[#]; Xiao, S. N.; Zhu, T. & Wang, F.
State Key Laboratory of Traction Power, Southwest Jiaotong University, Chengdu, 610031, China
E-Mail: gwyang@home.swjtu.edu.cn ([#] Corresponding author)

Abstract
The *Fa–N* curves of ring-welded specimens were obtained by performing tensile-shear fatigue tests to develop a method for accurate prediction of the fatigue lives of ring-welded joints. The correlation, affecting factors, and survival rate of the *Fa–N* curve were analysed. It was observed that unified *S–N* curve was required to improve the poor correlation and non-universality deficiencies of the *Fa–N* curve. Eight types of finite-element models of a ring-welded joint were established and the C_BAR umbrella finite-element model was used as a simplified model of the ring-welded joint. Subsequently, the Δ*S–N* and *P*–Δ*S–N* curves of the ring-welded specimens were obtained. A comparison with the *Fa–N* curve indicated that the Δ*S–N* and *P*–Δ*S–N* curves were comparatively relevant and universal. Finally, three extrapolation fatigue-assessment methods were proposed to predict the fatigue life of ring-welded joints with unknown plate thicknesses. A comparative analysis was conducted and it was concluded that the prediction using the interpolation extrapolation method had the highest accuracy. The research provides guidance for fatigue-life prediction of ring-welded joints in engineering application.
(Received in January 2022, accepted in March 2022. This paper was with the authors 1 month for 1 revision.)

Key Words: Ring-Welded Joints, Δ*S–N* Curve, *Fa–N* Curve, Finite Element Simulation, Fatigue Evaluation

1. INTRODUCTION

Welded joints are obtained by joining two or multiple parts by the process of welding. Welding processes can be divided into different types depending upon the shape formed by the parts. A few examples include ring welding, fillet welding, plug welding, spot welding, and butt welding [1]. Ring welding is a prominent type of joint welding and it is used as a supplementary welding method. It involves forming a round hole of a certain diameter in an outer plate and performing gas-shielded welding along the annular overlapping areas of the two plates in the round hole [2]. Ring-welded joints exhibit small welding deformation. Therefore, ring welding or plug welding is used as a supplementary welding method in stainless-steel car bodies of rail vehicles where spot welding is difficult to perform. Vehicles are subjected to dynamic loads such as self-excited vibration of the equipment and track irregularities during their operation [3, 4]. A significant stress concentration can develop around the solder joint under such loads due to the notch effect and welding defects of ring welding [5-7]. Therefore, ring-welded joints are prone to fatigue failure under dynamic loads and it is crucial to study the fatigue characteristics of ring-welded joints.

Significant advancements have been observed in the fatigue-life assessment of spot-welded joints [8, 9]. However, only a few studies have investigated the fatigue-life assessment of ring-welded joints. Furthermore, ring-welded joints have not been mentioned in a few welding standards. Ring-welded and spot-welded joints have similar structural and macroscopic mechanical characteristics. However, the bonding areas of the two joints are different at the solder joint. The bonding area in the case of ring welding is the projected area of the fillet-welded seam on the non-perforated plate, whereas the bonding area in the case of spot welding is the projected area of the weld nugget on the plate [2]. Therefore, the fatigue-life assessment of ring-welded joints is based on the similar principle as that used for spot-welded joints.

Baek et al. [10] investigated the welding residual stress generated by thermal cycling during plug/ring welding through a nonlinear finite-element analysis and an experimental drilling method. Additionally, they obtained the modified Goodman equation, stress amplitude $(\sigma_a)_R$, and $(\sigma_a)_R$–fatigue life (N_f) curves for the ring-welded joints. Wen [2] proposed a method to predict the fatigue lives of ring-welded joints based on the theory of fracture mechanics. Subsequently, Liu [11] calculated the structural stress in a ring-welded joint using the damage rules of the weld toe and provided a simplified method to calculate the fatigue-crack growth life. Shang [12] observed that when the beam element model with section properties was used to simulate a ring-welded joint, the error was small and it satisfied the accuracy requirements. Wang [13] observed that the failure of these joints was caused by a fatigue failure at the weld nugget and obtained the *S*–*N* curves of ring-welded joints under tension and shear loads. Yang et al. [14] optimized a ring-welding *S*–*N* curve using the quasi-Newton method and demonstrated that the correlation coefficient of the *S*–*N* curve was not dependent upon the hole diameter or plate thickness. Additionally, researchers have performed numerical investigations on the process of ring welding [15], and the temperature and residual stress fields in ring-welded joints [16]. Furthermore, research has been conducted to analyse the microstructures and mechanical properties of ring-welded joints [17], and examine the evolution of corrosion cracking of ring-welded joints [18].

The abovementioned studies have significantly contributed to the development of a calculation method for the residual stress, load amplitude–life (*Fa*–*N*) curve, fatigue-crack growth, finite-element simulation, and stress–life (*S*–*N*) curve under tensile shear load of ring-welded joints. However, the *Fa*–*N* curves vary with the input parameters, i.e., load mode, plate thickness, and weld nugget diameter in the experiments. The process is time-consuming, laborious, and uneconomical if the experimental research is performed for each form, thus limiting the engineering application of ring-welded joints [8]. At present, the research conducted on the fatigue-life characteristics of ring-welded joints and fatigue-assessment methods is inadequate. Therefore, it is crucial to compare the *Fa*–*N* and *S*–*N* curves of ring-welded joints with that of different survival rates to obtain a universal fatigue-life evaluation method for ring welding which is convenient for predicting the fatigue life of ring-welded structures.

In the present study, the *Fa*–*N* curve for ring-welded joints was obtained through tensile-shear fatigue tests. The stress range–life (ΔS–N) curve of the ring-welded specimens was obtained based on the equivalent structural stress method and the C_BAR umbrella finite-element model. The affecting factors and applicability of the two curves were compared and analysed to obtain a universal fatigue-life prediction curve. Finally, an extrapolation fatigue-assessment method with engineering significance for ring-welded joints was developed.

2. RING-WELDING RESEARCH METHOD

2.1 *Fa*–*N* curve of ring-welded joint

In this study, tensile-shear fatigue tests were performed on ring-welded specimens to determine the fatigue lives of ring-welded joints. SUS301L was selected as the material for the specimens because it is commonly used to manufacture rail vehicles. Some welding processes of stainless-steel car bodies of rail vehicles consists of ring-welded joints. The tests were performed using a Swiss RUMUL high-frequency fatigue tester. The loading frequency gradually decreased with crack propagation in the specimens and the frequency range was 60 – 90 Hz. A photograph and the schematic of the ring-welded specimen and test fixture are shown in Fig. 1. An auxiliary plate was welded at the edge of the clamped specimen to ensure a uniform clamping thickness and force on the welded joint. This was performed to prevent loading eccentricity due to the different thicknesses of the specimens during the test. The parameters of the specimens are presented in Table I. The fracture life of the specimen recorded by the fatigue tester was regarded as the fatigue life.

Table I: Geometric parameters and load ratios of the ring-welded specimens.

Type	t_1 (mm) **(perforated plate)**	t_2 (mm)	l (mm)	Φ (mm)	W (mm)	**Load ratio** R	**Number of specimens**
A	5	8	75	25	75	0.1	22
	5	8	75	25	75	0.5	3
B	1.5	2	40	14	40	0.1	24
	1.5	2	40	14	40	0.5	6
C	4	2	60	20	60	0.1	16
	4	2	60	20	60	0.3	4
	4	2	60	20	60	0.5	6
D	2	1.5	40	12	40	0.1	10
	2	1.5	40	12	40	0.5	6
E	2	1.5	40	14	40	0.1	25
	2	1.5	40	14	40	0.5	6
F	3	4	40	14	40	0.1	23
	3	4	40	14	40	0.5	3

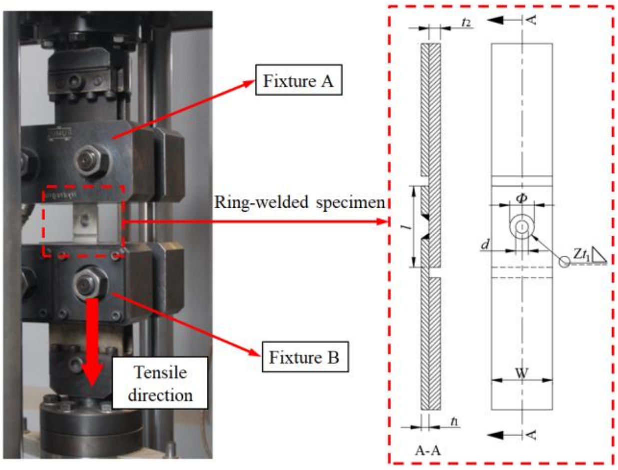

Figure 1: Photograph and schematic of the ring-welded specimen and test fixture.

Cracks were observed in the fractured specimens. The two plates of the specimens cracked under a high load as shown in Fig. 2 a. The cracks originated from the weld nugget and expanded to both sides of the base metal. In contrast, the specimens only exhibited cracks on the perforated plate under a low load, as shown in Fig. 2 b. These cracks originated from the weld nugget and expanded to both sides of the base metal.

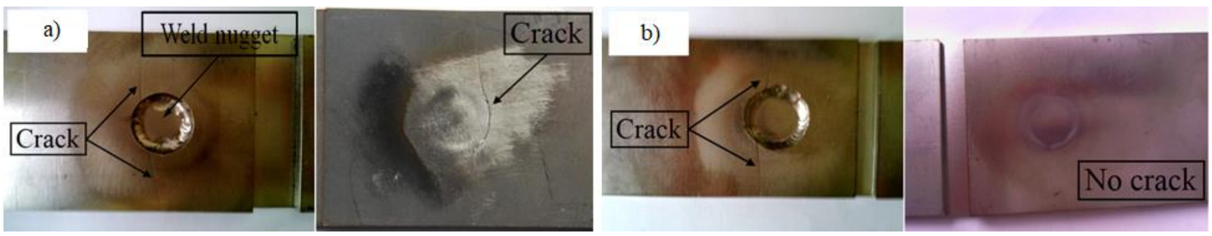

Figure 2: a) Fatigue crack under a high load (t: 4 + 2 mm, Φ20 mm), b) fatigue crack under a low load (t: 2 + 1.5 mm, Φ14 mm), c) fractured specimen under a high load (t: 5 + 8 mm, Φ25 mm).

The Fa–N curves of the ring-welded specimens were constructed according to the test loads and tensile-shear fatigue lives of the specimens as shown in Fig. 3. The data were highly dispersed and the curves exhibited a weak correlation after distinguishing the plate thickness

(t), weld-nugget diameter (Φ), load ratio (R), and the perforated plate. The square of the correlation coefficient (R^2) for the overall Fa–N curve was 0.1426, indicating that the correlation between Fa and N for the ring welding was weak. Therefore, the Fa-N curve fitted appropriately only for the ring-welded joints with the same structure. When predicting the fatigue lives of different ring-welded joints, fatigue tests had to be performed for each structure.

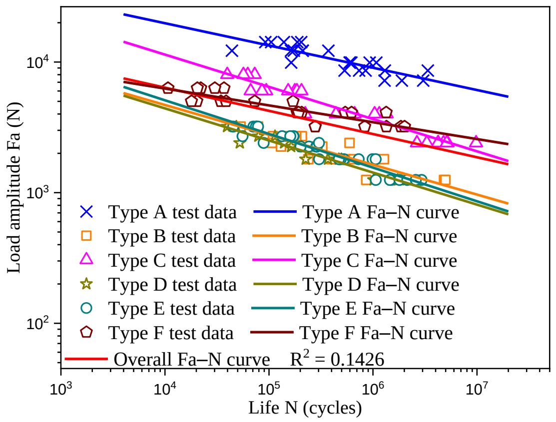

Figure 3: Fa–N curves.

2.2 Factors affecting the *Fa–N* curve

The comparison between the Fa–N curves is presented in Table II. A comparison between the deviation of Type II and Type I demonstrated that Φ and the choice of the perforated plate had the least effect on the Fa–N curve, which was followed by R and t. A comparison of the deviation of Type III and Type I demonstrated that t and the choice of the perforated plate were least affected by the parameters, followed by Φ and R. The analysis demonstrated that different ring-welded structures had different Fa–N curves. The Fa–N curves under the same set of parameters exhibited a good correlation and the curves under different parameters exhibited significant deviation. Therefore, it is necessary to individually perform fatigue tests for each structure while using the Fa–N curves to evaluate the fatigue of ring-welded joints. This exhibited a lack of universal applicability of the Fa–N curves.

Table II: Comparison between Fa–N curves and the squares of the correlation coefficients (R^2).

Influencing parameter	**Type**	***Fa–N* curve: lg(*Fa*) = *a* × lg(*N*) + *b***			**Deviation from the overall *Fa–N* curve** (%)			**Deviation of Type II relative to Type I** (%)			**Deviation of Type III relative to type I** (%)		
		A	***b***	***R*²**	**Δ*a***	**Δ*b***	**Δ*R*²**	**Δ*a***	**Δ*b***	**Δ*R*²**	**Δ*a***	**Δ*b***	**Δ*R*²**
t	Type I	–0.26	4.75	0.94	45.58	5.23	556.10	–11.69	1.17	–42.89	–3.58	–1.56	–4.35
	Type II	–0.23	4.69	0.53	28.57	4.00	274.68						
	Type III	–0.25	4.68	0.89	40.36	3.59	527.56						
Φ	Type I	–0.26	4.75	0.94	45.58	5.23	556.10	–1.45	–0.67	–0.09	–3.91	0.12	–35.92
	Type II	–0.25	4.72	0.93	43.46	4.52	555.54						
	Type III	–0.25	4.76	0.60	39.88	5.36	320.41						
Load ratio *R*	Type I	–0.26	5.16	0.98	48.11	14.36	584.92	–6.14	–2.28	–4.80	–40.93	–14.48	–89.10
	Type II	–0.25	5.04	0.93	39.01	11.75	552.03						
	Type III	–0.16	4.41	0.11	–12.52	–2.20	–25.32						
Perforated plate	Type I	–0.26	4.75	0.94	45.58	5.23	556.10	–5.07	–1.47	–0.95	–3.58	–1.56	–4.35
	Type II	–0.25	4.68	0.93	38.20	3.68	549.86						
	Type III	–0.25	4.68	0.89	40.36	3.59	527.56						
Overall *Fa-N* curve		–0.18	4.51	0.14	/								

Note: Type I implies that the affecting parameters and the other parameters remain unchanged. Type II implies that the affecting parameters change while the other parameters remain unchanged. Type III implies that the affecting parameters remain unchanged while the other parameters change.

2.3 *P–Fa–N* curve of ring-welded joints

The *Fa–N* curves can only consider the effect of the survival rate for the same ring-welded joint because the loads borne by different ring-welded joints were different. The probabilistic *Fa–N* (*P–Fa–N*) curves of each ring-welded joint are presented in Fig. 4. The data points recorded were included in the *Fa–N* curve with a 99.9 % survival rate and the dispersion of the data points was small. However, the survival rate was only meaningful for ring-welded specimens with the same structure because different structures produced different *Fa–N* and *P–Fa–N* curves. *Fa–N* curves and complex finite-element models are used in the fatigue analysis of ring-welded joints. However, ring-welded joints with different values of *t* and *Φ*, and additional varying parameters are present in actual engineering structures. Performing fatigue tests or finite-element modelling for each structure is time-consuming, laborious, and counterproductive. Therefore, it is crucial to simplify the ring-welding fatigue analysis method by normalizing different *Fa–N* curves, establishing a ring-welding *S–N* curve that comprehensively considers the geometric parameters and load ratios, and developing a *P–S–N* curve suitable for the engineering application under consideration.

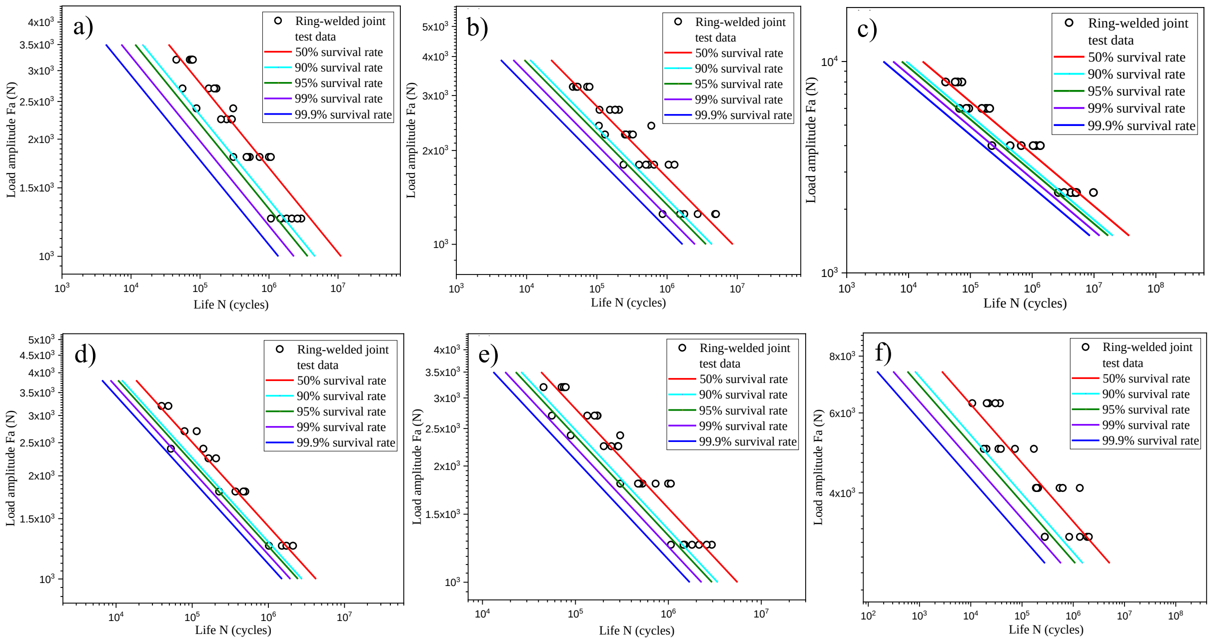

Figure 4: *P–Fa–N* curves: a) Type A, b) Type B, c) Type C, d) Type D, e) Type E, f) Type F.

3. SIMULATION MODELLING AND RESULTS

3.1 Simplification of the ring-welding model

There are various models used for finite-element simulation of ring-welded joints and the main eight types are shown in Fig. 5. These models were established using HyperMesh software. The mesh size of the base metal was 2 mm and the mesh at the weld nugget was relatively fine, with a size of 0.5 mm. The load and boundary conditions were consistent with that of the test. One end of the specimen was fully constrained, while the other end was connected to the rbe2 rigid element and released the degree of freedom of the load direction. The modelling method and characteristics of each ring-welding finite-element model are presented in Table III.

Table III: Modelling method and characteristics of each ring-welding finite-element model.

Model	Element type		Simulation accuracy	Modelling time	Complexity level
	Base metal	**Weld nugget**			
a	Hexahedral element (SOLID)	Hexahedral element (SOLID)	Highest	Longest	Highest
b	Shell element	Hexahedral element (SOLID) and shell element	Moderate	Long	High
c	Shell element	Shell element	Moderate	Moderate	Low
d	Shell element	Elastic beam CBAR	High	Shortest	Lowest
e	Shell element	Multi-elastic beam (M_CBAR) with a triangular section and a fully restrained multi-rigid beam (M_Rigid)	High	Long	Medium
f	Shell element	Displacement-constrained multi-rigid beam (M_Rigid)	Moderate	Moderate	Medium
g	Shell element	Fully constrained multi-rigid beam (M_Rigid)	Moderate	Moderate	Medium
h	Shell element	Hexahedral element (SOLID) and flexible connection element RBE3	Low	Long	Medium

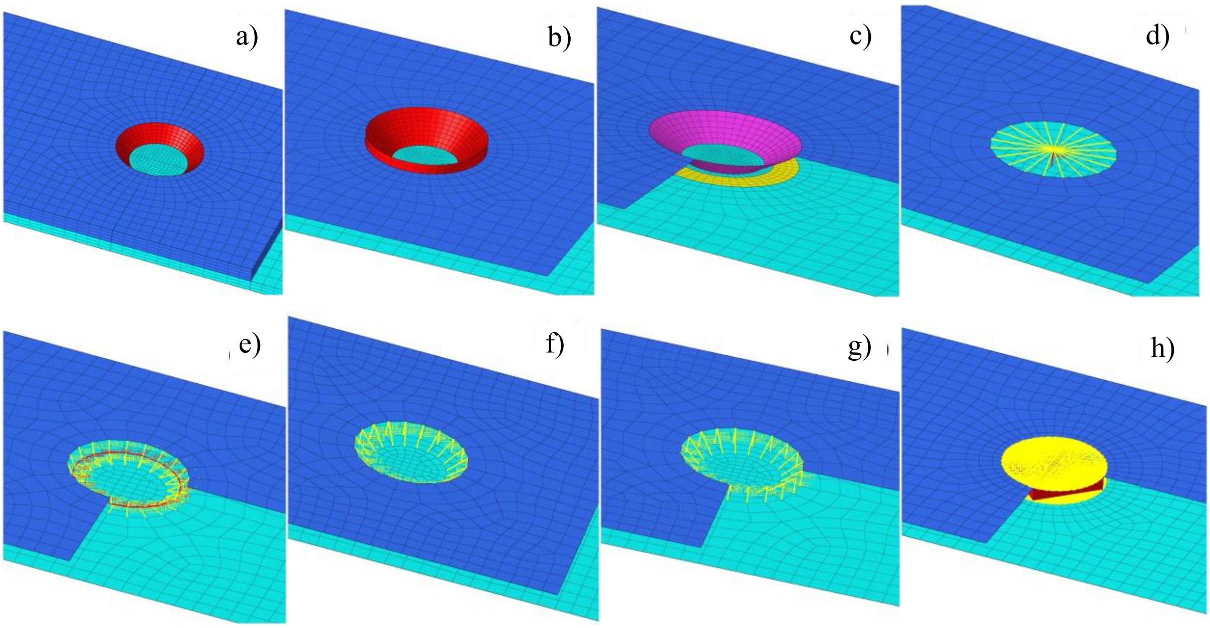

Figure 5: Conventionally used ring-welding finite-element models: a) solid model, b) solid shell model, c) shell model, d) CBAR umbrella model, e) multi-beam element model, f) rigid beam coupled articulation model, g) rigid beam coupled fully constrained model, h) surface contact model (ACM2).

Nastran software was used to simulate the ring-welded finite-element models. A comparison between the simulation results for the different models is presented in Table IV (the maximum load was 2778 N and the stress ratio was 0.1). The analysis results for the solid model in the table were considered as a benchmark and were compared with that of the results obtained for the remaining models. The solid shell and shell models were not able to construct and reflect the accurate stiffness of the weld nugget, which introduced errors in the simulation results. Hence, the simulation accuracy was moderate. The force applied by the surface contact model (ACM2) to the hexahedral element distributed on the shell element nodes was dependent upon the weighting factor assigned to the shell element nodes by RBE3. The difference in the weighting factors resulted in non-uniform force distribution to the shell elements of the upper and lower welded plates, resulting in low simulation accuracy. The C_BAR umbrella and multi-beam element models with triangular section properties accurately simulated the stiffness and vibration fatigue characteristics of the weld nugget. The rigid beam coupled articulation and coupled fully constrained model accurately simulated the stiffness of the weld area. However, the weld area was rigid, resulting in a relatively large fatigue-life error.

A comparison between the eight types of ring-welding models revealed that the C_BAR umbrella model (single beam model) had advantages such as high simulation accuracy and short modelling time. According to the requirements of batch processing and the solution accuracy of the solder joint in engineering, the C_BAR umbrella model (single beam model) was selected as the simplified model for the ring-welded joint in this study.

Table IV: Comparison of simulation results of ring-welding finite-element models.

Finite-element model	**Stress amplitude** (MPa)	**Relative error with solid model** (%)	**Fatigue life** (cycle)	**Relative error with solid model** (%)	**First-order natural frequency** (Hz)	**Relative error with solid model** (%)
Solid model	97.49	/	202600	/	151.30	/
Solid shell model	113.19	16.10	256800	26.75	139.80	–7.60
Shell model	115.03	17.99	254000	25.37	145.20	–4.03
CBAR umbrella model (Single beam)	102.01	4.64	183400	–9.48	145.40	–3.90
Multi-beam element model	99.20	1.75	246900	21.87	144.50	–4.49
Rigid beam coupled articulation model	98.49	1.03	356000	75.72	147.40	–2.58
Rigid beam coupled fully constrained model	106.81	9.56	274200	35.34	149.50	–1.19
Surface contact model (ACM2)	113.14	16.05	396200	95.56	187.90	24.19

3.2 Equivalent structural stress

The maximum principal stress on the annular weld nugget section of the ring-welded joint was derived on the basis of the equivalent structural stress calculation method of spot welding [19] as shown in Fig. 6. The equations used to calculate the equivalent structural stress of the ring-welded joint under a tensile-shear load are as follows [13, 14].

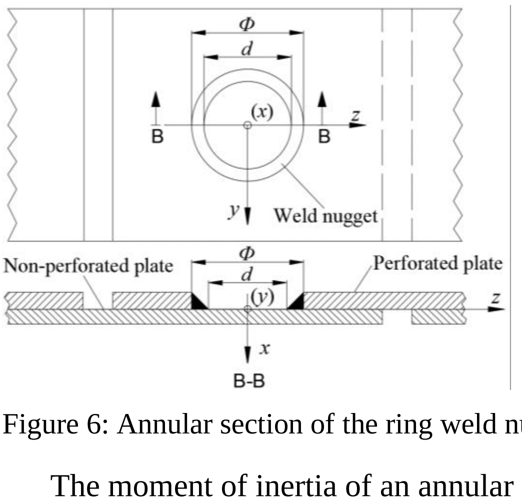

Figure 6: Annular section of the ring weld nugget.

The moment of inertia of an annular section is expressed as:

$$I_y = I_z = \frac{\pi(\Phi^4 - d^4)}{64} \tag{1}$$

$$\tau_{\max}(F_{x3}) = \frac{8F_{x3}}{\pi(\Phi^4 - d^4)} \tag{2}$$

$$\tau_{\max}(F_{y3}) = \frac{8F_{y3}}{\pi(\Phi^4 - d^4)} \tag{3}$$

When $F_{z3} > 0$,

$$\sigma(F_z) = \frac{4F_z}{\pi(\Phi^4 - d^4)} \tag{4}$$

When $F_{z3} \leq 0$,

$$\sigma(F_{z3}) = 0 \tag{5}$$

$$\sigma_{\max}(M_{z3}) = \frac{32M_{z3}\Phi}{\pi(\Phi^4 - d^4)} \tag{6}$$

$$\sigma_{\max}(M_{y3}) = \frac{32M_{y3}\Phi}{\pi(\Phi^4 - d^4)} \tag{7}$$

Therefore, the structural stress at the weld nugget of the ring-welded specimen can be expressed as:

$$\tau = \tau_{\max}(F_{x3})\sin^2\theta + \tau_{\max}(F_{y3})\cos^2\theta \tag{8}$$

$$\sigma = \sigma(F_{z3}) + \sigma_{\max}(M_{x3})\sin\theta - \sigma_{\max}(M_{y3})\cos\theta \tag{9}$$

$$\sigma_{1,3} = \frac{\sigma}{2} \pm \sqrt{\left(\frac{\sigma}{2}\right)^2 + \tau^2} \tag{10}$$

4. ANALYSIS OF SIMULATION RESULTS

4.1 *S–N* curve of ring-welded joint

The following steps were performed to construct the *S–N* curves of ring-welded joints. Initially, the CBAR umbrella finite-element model was developed for the ring-welded specimens mentioned in Table I. Each type of the combined loading form of *R* and the load amplitude (*Fa*) was simulated in the form of the maximum and minimum loads (F_{max} and F_{min}) in the finite-element model. Subsequently, the values of force and moment of the beam element obtained by the simulation were substituted into Eqs. (1) to (10) to determine the equivalent structural stress (*S*) of each ring-welded specimen. Finally, the data were fitted in a double-logarithmic coordinate system using the least-squares method by considering the equivalent structural stress range ΔS as the ordinate and the fatigue life *N* as the abscissa. The ring-welding ΔS–*N* curve considering the geometric parameters and load ratios was obtained as shown in Fig. 7 a. The true vs. predicted life curves are shown in Fig. 7 b.

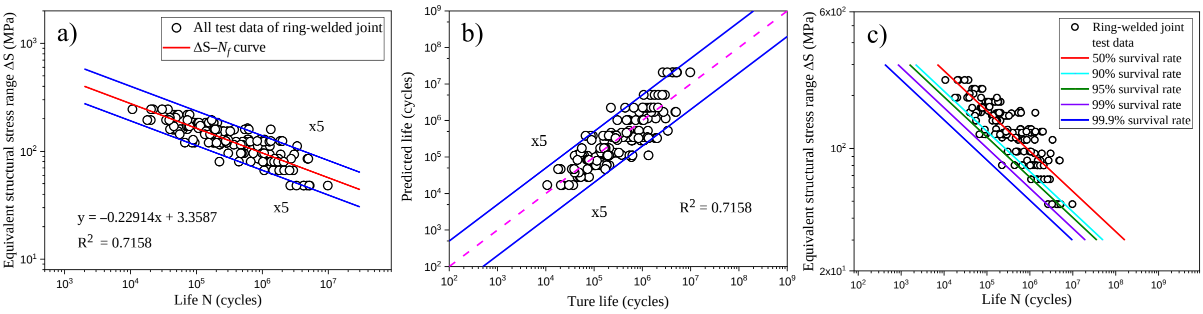

Figure 7: Curves: a) ΔS–*N* curve of the ring-welded joint, b) true vs. predicted life curves, c) *P*–ΔS–*N* curves.

Conventionally, five times the lifespan (hereinafter referred to as "5×lifespan") is used to evaluate the *S–N* curve. If the data points are within 5×lifespan, the *S–N* curve is considered to have a high correlation [20, 21]. It can be observed from Fig. 7 b that the ring-welding data points were within the 5×lifespan. Additionally, the R^2 value was significantly improved relative to the *Fa–N* curve, indicating that the structural stress range ΔS had a good correlation with the fatigue life *N* and the predicted life was relatively close to the true life of the test.

4.2 Factors affecting the *S*–*N* curve

The comparison results for the Δ*S*–*N* curves are presented in Table V. The correlation of each Δ*S*–*N* curve was significantly improved relative to the *Fa*–*N* curve as indicated by Tables II and V. A comparison between the deviations of Type II and Type I demonstrated that *Φ* and *R* had the least effect on the Δ*S*–*N* curve, followed by the choice of the perforated plate, while *t* had a significant effect on the Δ*S*–*N* curve. A comparison between the deviations of Type III and I demonstrated that *t* and the choice of the perforated plate had the least effect, followed by *R*. *Φ* had a significant effect on the Δ*S*–*N* curve.

It was concluded that the overall correlation of the Δ*S*–*N* curve was relatively good. Therefore, the overall effect of the parameters on the curve was relatively small and different ring-welded structures had approximately identical Δ*S*–*N* curves. The Δ*S*–*N* curve of the ring weld, which comprehensively considered the geometric parameters and load ratios, had a good correlation and it can be used to predict the fatigue lives of different ring-welded structures. Therefore, it can be inferred that the fatigue assessment of ring-welded structures did not require fatigue tests for each structure. Hence, the Δ*S*–*N* curve had a greater universal applicability compared with that of the *Fa*–*N* curve.

Table V: Comparison between the Δ*S*–*N* curves and squares of the correlation coefficients (R^2).

Influencing parameter	Type	**Δ*S*-*N* curve: lg(Δ*S*) = *a* × lg(*N*) + *b***			**Deviation from the overall Δ*S*–*N* curve** (%)			**Deviation of Type II relative to Type I** (%)			**Deviation of Type III relative to Type I** (%)		
		A	***b***	R^2	Δ*a*	Δ*b*	ΔR^2	Δ*a*	Δ*b*	ΔR^2	Δ*a*	Δ*b*	ΔR^2
t	Type I	–0.26	3.48	0.94	12.82	3.49	30.71	–21.70	–7.32	–24.40	–0.82	–0.22	–3.00
	Type II	–0.20	3.22	0.71	–11.66	–4.08	–1.19						
	Type III	–0.26	3.47	0.91	11.90	3.26	26.78						
Φ	Type I	–0.26	3.48	0.94	12.82	3.49	30.71	1.84	1.07	0.36	–18.57	–5.72	–23.98
	Type II	–0.26	3.51	0.94	14.90	4.60	31.18						
	Type III	–0.21	3.28	0.71	–8.13	–2.43	–0.64						
Load ratio *R*	Type I	–0.26	3.46	0.98	14.78	3.12	36.45	–6.14	–3.40	–4.80	–14.97	–3.35	–23.56
	Type II	–0.25	3.35	0.93	7.73	–0.39	29.90						
	Type III	–0.22	3.35	0.75	–2.40	–0.33	4.30						
Perforated plate	Type I	–0.26	3.48	0.94	12.82	3.49	30.71	–4.42	–0.22	–14.44	–0.82	–0.22	–3.00
	Type II	–0.25	3.47	0.80	7.83	3.26	11.83						
	Type III	–0.26	3.47	0.91	11.90	3.26	26.78						
Overall Δ*S*–*N* curve		–0.23	3.36	0.72	/								

4.3 *P*–Δ*S*–*N* curves of ring-welded joints

In contrast to the *Fa*–*N* curve, the Δ*S*–*N* curve did not consider the effect of the load and survival rate for different ring-welded joints. The *P*–Δ*S*–*N* curves of ring-welded joints are presented in Fig. 7 c. It can be observed that the data points were included in the Δ*S*–*N* curve with a 99.9 % survival rate and the dispersion of the data points was small. A comparison between Figs. 4 and 7 c demonstrated that the dispersion of the data of the *P*–Δ*S*–*N* curve, which considered the geometric parameters and *R*, was not significantly different from that of the *P*–*Fa*–*N* curve. However, the *P*–Δ*S*–*N* curve can be used to predict the fatigue lives of different ring-welded structures. Therefore, the fatigue assessment of ring-welded structures does not require fatigue tests for each structure and the *P*–Δ*S*–*N* curve had a greater universality compared with that of the *P*–*Fa*–*N* curve.

5. FATIGUE LIFE EXTRAPOLATION METHOD

Φ and the choice of the perforated plate had the least effect on the *Fa*–*N* curve as indicated by Table II. Hence, they can be neglected. *t* had a significant effect on the *Fa*–*N* curve and it cannot be neglected. Therefore, in order to predict the fatigue life of ring-welded joints with unknown *t*, it is necessary to provide an extrapolation fatigue-assessment method to extrapolate the fatigue lives of ring-welded joints with unknown *t* values according to the test data of the existing *t* values. According to the fatigue-test data of Type B (*t*: 1.5 + 2 mm; *R* = 0.1) and Type C (*t*: 4 + 2 mm, *R* = 0.1), the following three extrapolation methods were used to extrapolate the data of *t*: 3 + 2 mm.

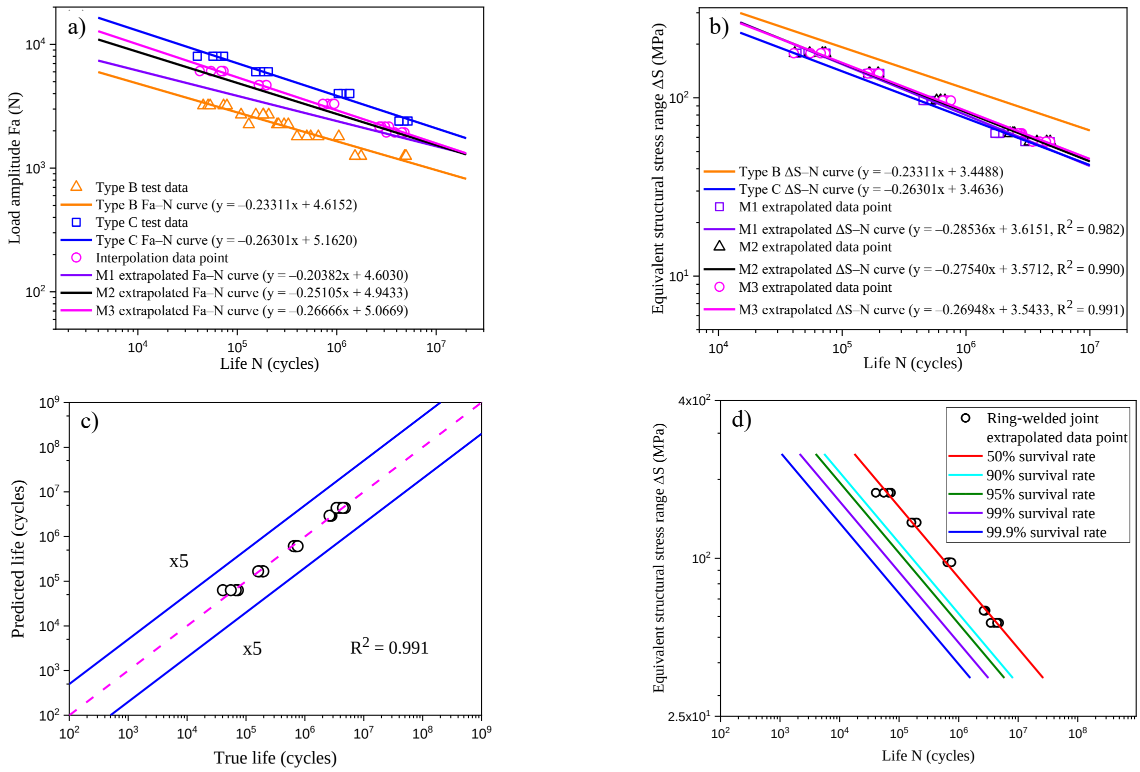

Figure 8: Extrapolation curve for *t*: 3 + 2 mm: a) extrapolated *Fa–N* curves, b) extrapolated Δ*S–N* curves, c) true vs. predicted life curves (M3 extrapolation method), d) *P*–Δ*S–N* curves (M3 extrapolation method).

1) Fitting extrapolation method (M1)

The extrapolated *Fa-N* curve of unknown *t* was obtained using the existing ring-welding test data of two *t*-combinations.

2) Curve extrapolation method (M2)

According to the ring-welding *Fa–N* curve of the two existing *t*-combinations, the slope *a* and intercept *b* were linearly interpolated to obtain the slope *a* and intercept *b* of the extrapolated *Fa–N* curve of unknown *t*.

3) Interpolation extrapolation method (M3)

Considering *t* as a variable, linear interpolation was performed on the test data of the existing two *t*-combinations to obtain the data of the unknown *t*. The data obtained by linear interpolation were fitted by the least-squares method and the extrapolated *Fa–N* curve was obtained.

The *Fa–N* curves obtained using the three extrapolation methods are presented in Fig. 8 a. In the test range, the three extrapolated *Fa–N* curves of unknown *t* were located between the *Fa–N* curves of the existing *t* and the three curves exhibited differences. According to the equivalent structural stress range Δ*S* and the extrapolated fatigue life *N*, the extrapolated Δ*S–N* curves were obtained as shown in Fig. 8 b. The three extrapolated Δ*S–N* curves of unknown *t* in the test range were located between the Δ*S–N* curves of the existing *t* and the three curves tended to converge, indicating that the Δ*S–N* curve was the result of normalizing different

Fa–N curves, with higher correlation and universality. A comparison of the three extrapolation methods demonstrated that the Δ*S–N* curve obtained via the M3 extrapolation method had the highest correlation, followed by M2 and then M1. The true vs. predicted life curves obtained via the M3 extrapolation method are shown in Fig. 8 c, and the *P–*Δ*S–N* curves are shown in Fig. 8 d. The data points were present within 5× lifespan, and the R^2 value was large. The data points were included in the Δ*S–N* curve with a 90 % survival rate and the dispersion of the data points was small.

In summary, the correlation of Δ*S-N* curve of ring-welded joints was better than that of *Fa-N* curve. Among the three extrapolation fatigue-assessment methods, the interpolation extrapolation method had the best effect on the fatigue life prediction of ring-welded joints, which provide guidance for engineering applications.

6. CONCLUSION

Fatigue tests and finite-element simulations of a ring-welded joint were performed to obtain the Δ*S–N* curves. Additionally, the extrapolation fatigue-assessment methods for ring welding were studied on the basis of the structural stress method. The following conclusions are obtained on the basis of the results:

1) The *Fa–N* curve of the ring-welded specimens exhibited a poor correlation and the effects of different parameters on the curve significantly varied. The curve considered only the effect of the survival rate for the same structure. Therefore, the *Fa–N* curve was not universal.

2) The C_BAR umbrella model for the ring-welding simulation model had advantages such as high simulation accuracy and short modelling time. This model can be used as a simplified model for ring-welded joints to extract the structural stress of the weld nugget.

3) The Δ*S–N* curve of ring welding obtained via the equivalent structural stress method was $\lg(\Delta S) = -0.22914 \lg(N) + 3.3587$, which had a good correlation and the differences in the structures had negligible effect on the Δ*S–N* curve. The curve considered the effect of the survival rate for different ring-welded joints. Therefore, it exhibited a greater universality compared with that of the *Fa–N* curve.

4) Three extrapolation fatigue-assessment methods for ring-welded joints were proposed. A comparison indicated that the interpolation extrapolation method exhibited optimum results and can provide guidance for engineering applications.

Owing to the limited amount of test data, some of the data were dispersive and did not provide accurate solutions; therefore, supplementary experiments are needed to improve the results. In the future, the effects of residual stress on the fatigue lives of ring-welded joints should be further studied.

ACKNOWLEDGEMENT

This work was supported by the National Natural Science Foundation of China (No. 51675446), the Independent Subject of State Key Laboratory of Traction Power (2019TPL-T13).

REFERENCES

[1] Kolpakov, A. G.; Rakin, S. I. (2018). Estimation of stress concentration in a welded joint formed by explosive welding, *Journal of Applied Mechanics and Technical Physics*, Vol. 59, No. 3, 569-575, doi:10.1134/S0021894418030227

[2] Wen, M. F. (2012). *Research on Fatigue Properties and Life Prediction of Ring Welding Joints for Stainless Steel Carbody*, Southwest Jiaotong University, Chengdu (in Chinese)

[3] Wang, Q. S.; Zhou, J. S.; Gong, D.; Wang, T. F.; Chen, J. X.; You, T. W.; Zhang, Z. F. (2020). The influence of the motor traction vibration on fatigue life of the bogie frame of the metro vehicle, *Shock and Vibration*, Vol. 2020, Paper 7385861, 11 pages, doi:10.1155/2020/7385861

[4] Zhang, D. W.; Zhai, W. M.; Wang, K. Y. (2017). Dynamic interaction between heavy-haul train and track structure due to increasing axle load, *Australian Journal of Structural Engineering*, Vol. 18, No. 3, 190-203, doi:10.1080/13287982.2017.1363126

[5] Dunder, D.; Samardzic, I.; Simunovic, G.; Konjatic, P. (2020). Steel weldability investigation by single and double-pass weld thermal cycle simulation, *International Journal of Simulation Modelling*, Vol. 19, No. 2, 209-218, doi:10.2507/IJSIMM19-2-510

[6] Duan, B.; Wang, J. C.; Lu, Z. H.; Zhang, G. X.; Zhang, C. H. (2018). Parameter analysis and optimization of the rotating arc NG-GMAW welding process, *International Journal of Simulation Modelling*, Vol. 17, No. 1, 170-179, doi:10.2507/IJSIMM17(1)CO4

[7] Wang, Q. D.; Ji, B. H.; Gao, T.; Fu, Z. Q. (2021). Effective-notch-stress-based fatigue evaluation of rib-deck welds integrating the full-range *S–N* curve concept, *Journal of Constructional Steel Research*, Vol. 179, Paper 106541, doi:10.1016/j.jcsr.2021.106541

[8] Yang, L.; Yang, B.; Yang, G. W.; Xiao, S. N.; Zhu, T.; Wang, F. (2020). S-N curve and quantitative relationship of single-spot and multi-spot weldings, *International Journal of Simulation Modelling*, Vol. 19, No. 3, 482-493, doi:10.2507/IJSIMM19-3-CO11

[9] Yang, L.; Yang, B.; Yang, G. W.; Xiao, S. N.; Zhu, T.; Wang, F. (2020). A comparative study of fatigue estimation methods for single-spot and multispot welds, *Fatigue & Fracture of Engineering Materials & Structures*, Vol. 43, No. 6, 1142-1158, doi:10.1111/ffe.13185

[10] Baek, S. Y.; Bae, D. H.; Kim, H. (2008). Fatigue design for plug/ring type gas welded joints of sts301l including welding residual stresses, *International Journal of Automotive Technology*, Vol. 9, No. 6, 729-734, doi:10.1007/s12239-008-0086-6

[11] Liu, W. (2014). *Research on Fatigue Life Prediction of Ring Welding Joints*, Southwest Jiaotong University, Chengdu (in Chinese)

[12] Shang, L. Y. (2012). *Study on Fatigue Assessment Numerical Method for Plug and Ring Welding*, Southwest Jiaotong University, Chengdu (in Chinese)

[13] Wang, F. (2018). *Research on Equivalent Stress Method of Spot Welding and Ring Welding*, Southwest Jiaotong University, Chengdu (in Chinese)

[14] Yang, G. W.; Che, C. J.; Yang, B.; Zhu, T.; Wang, F.; Wang, J. J. (2019). Optimization research on S-N curve of ring welding structure based on structural stress method, *Fatigue & Fracture of Engineering Materials & Structures*, Vol. 42, No. 10, 2207-2219, doi:10.1111/ffe.13023

[15] Miao, Z. Y.; Kong, F. Y.; Liu, H. (2016). Numerical simulation of residual stress in ring welding joint of T91 pipeline steel pipe based on SYSWELD, *Hot Working Technology*, Vol. 45, No. 17, 156-160, doi:10.14158/j.cnki.1001-3814.2016.17.044

[16] Liu, Y.-X.; Li, H.-Q.; Ma, Y.-L.; Xing, S.-H. (2011). Numerical simulation of Monel400 alloy welding temperature field and residual stress field, *Electric Welding Machine*, Vol. 41, No. 3, 75-78, doi:10.3969/j.issn.1001-2303.2011.03.018

[17] Li, R.; He, D. Q.; Wang, H. J. (2015). Microstructure and mechanical properties of friction stir welded joint of 7A09 Al alloy thick cylinder, *Hot Working Technology*, Vol. 44, No. 13, 27-29, doi:10.14158/j.cnki.1001-3814.2015.13.008

[18] Venugopal, A.; Narayanan, P. R.; Sharma, S. C. (2016). Evolution of microstructure and stress corrosion cracking behavior of AA2219 plate to ring weld joints in 3.5 Wt Pct NaCl solution, *Metallurgical and Materials Transactions A – Physical Metallurgy and Materials Science*, Vol. 47, No. 4, 1607-1620, doi:10.1007/s11661-016-3332-y

[19] Rupp, A.; Störzel, K.; Grubisic, V. (1995). *Computer Aided Dimensioning of Spot-Welded Automotive Structures*, SAE Technical Paper 950711, 13 pages, SAE International, Warrendale

[20] Kang, H.-T.; Wu, X.; Khosrovaneh, A. K.; Li, Z. (2017). Data processing procedure for fatigue life prediction of spot-welded joints using a structural stress method, *Fatigue and Fracture Test Planning, Test Data Acquisitions and Analysis – Symposia paper*, STP 1598, 198-211, doi:10.1520/STP159820160054

[21] Kang, H.; Barkey, M. E.; Lee, Y. (2000). Evaluation of multiaxial spot weld fatigue parameters for proportional loading, *International Journal of Fatigue*, Vol. 22, No. 8, 691-702, doi:10.1016/S0142-1123(00)00037-2